NMR IN BIOMEDICINE
NMR Biomed. 2008; **21**: 322–336
Published online 10 August 2007 in Wiley InterScience
(www.interscience.wiley.com) DOI:10.1002/nbm.1194

Gd(III)-EPTPAC$_{16}$, a new self-assembling potential liver MRI contrast agent: *in vitro* characterization and *in vivo* animal imaging studies†

Suzana Torres,[1] Maria I. M. Prata,[2] Ana C. Santos,[2] João P. André,[1] José A. Martins,[1] Lothar Helm,[3] Éva Tóth,[4] Maria L. García-Martín,[5] Tiago B. Rodrigues,[5,6] Pilar López-Larrubia,[5] Sebastián Cerdán[5] and Carlos F. G. C. Geraldes[6]*

[1]Centro de Química, Campus de Gualtar, Universidade do Minho, Braga, Portugal
[2]Instituto de Biofísica e Biomatemática, Faculdade de Medicina, Universidade de Coimbra, Coimbra, Portugal
[3]Laboratoire de Chimie Inorganique et Bioinorganique, Ecole Polytechnique Fédérale de Lausanne, EPFL-BCH, Switzerland
[4]Centre de Biophysique Moléculaire, CNRS, Orléans, France
[5]Instituto de Investigaciones Biomédicas ''Alberto Sols'', CSIC-UAM, Madrid, Spain
[6]Departamento de Bioquímica, Centro de RMN e Centro de Neurociências e Biologia Celular, Faculdade de Ciências e Tecnologia, Universidade de Coimbra, Coimbra, Portugal

Received 20 March 2007; Revised 28 May 2007; Accepted 3 June 2007

ABSTRACT: The recently reported amphiphilic chelate, [Gd(EPTPAC$_{16}$)(H$_2$O)]$^{2-}$, forms supramolecular aggregates in aqueous solution by self-assembly of the monomers with a relaxometrically determined critical micellar concentration (CMC) of 0.34 mM. The effect of sonication on the aggregate size was characterized by dynamic light scattering and relaxometry, indicating the presence of premicellar aggregates and an overall decrease in aggregate size and polydispersity upon sonication, slightly below the CMC. {[^{153}Sm](EPTPAC$_{16}$)(H$_2$O)}$^{2-}$ radiotracer was evaluated *in vivo* from γ scintigraphy and biodistribution in Wistar rats. It was found to depend strongly on the sample concentration, below or above the CMC, and its sonication, in a way that correlates with the effect of the same factors on the size of the aggregates formed in solution. Below CMC, the very large aggregates of the [^{153}Sm]$^{3+}$-labeled chelate were persistently and mainly taken up by the lungs, and also by the macrophage-rich liver and spleen. Sonication of this solution led to loss of the lung uptake. Above CMC, the metal chelate was mainly taken up by the liver, with very little uptake by the spleen and lungs. *In vivo*, dynamic contrast-enhanced (DCE)-MRI evaluation of the micellar [Gd(EPTPAC$_{16}$)(H$_2$O)]$^{2-}$ compound in Wistar rats showed a persistent hepatic positive-contrast effect in T_1-weighted images, qualitatively similar to the clinically established Gd^{III}-based hepatobiliary-selective agents. No enhancement effect was observed in the lungs because of the scarcity of mobile protons in this organ, despite the scintigraphic evidence of significant lung retention of the [^{153}Sm]$^{3+}$-labeled chelate at concentrations below the CMC. Copyright © 2007 John Wiley & Sons, Ltd.

KEYWORDS: MRI; contrast agents; gadolinium; liver targeting; self-assembly; micelles; dynamic light scattering; γ scintigraphy

INTRODUCTION

Gadolinium(III) chelates have been extensively used as paramagnetic contrast agents (CAs) for MRI (1–6). The first generation of MRI CAs, including [Gd(DOTA)(H$_2$O)]$^-$ (DOTA = 1,4,7,10-tetra-azacyclododecane-1,4,7,10-tetra-acetate) and [Gd(DTPA)(H$_2$O)]$^{2-}$ (DTPA = diethylenetriamine penta-acetate) among others, are

**Correspondence to:* C. F. G. C. Geraldes, Departamento de Bioquímica, Faculdade de Ciências e Tecnologia, Universidade de Coimbra, Apartado 3126, 3001-401 Coimbra, Portugal.
E-mail: geraldes@ci.uc.pt
†Supplementary Fig. S1 is available online in Supplementary Material.
Contract/grant sponsor: Foundation of Science and Technology, Portugal; *contract/grant numbers:* POCTI/QUI/47005/2002, SFRH/BD/5407/2001.
Contract/grant sponsor: FEDER.
Contract/grant sponsor: III Instituto de Investigação Interdisciplinar University of Coimbra, Portugal; *contract/grant number:* III/BIO/45/2005.
Contract/grant sponsor: Institute of Health Carlos III, Spain; *contract/grant number:* PIO051845.
Contract/grant sponsor: Ministry of Education and Science, Spain; *contract/grant numbers:* SAF 2004-0391, NAN2004-09125-C07-03.
Contract/grant sponsor: European Union; *contract/grant number:* LSCH-2004-503569.

Abbreviations used: CA, contrast agent; CCK, cholecystokinin; CMC, critical micellar concentration; DCE, dynamic contrast enhanced; DLS, dynamic light scattering; DTPA, diethylenetriamine penta-acetate; DOTA, 1,4,7,10-tetra-azacyclododecane-1,4,7,10-tetra-acetate; DOTP, 1,4,7,10-tetra-azacyclododecane-1,4,7,10-tetrakis(methylene phosphinate); EOB-DTPA, ethoxybenzyl-DTPA or *S*-[3,6,9-triaza-3,6,9-tris(carboxymethyl)-4-(4-ethoxybenzyl)-undecandicarboxylate]; H$_5$EPTPAC$_{16}$, (hydroxymethylhexadecanoyl ester) ethylenepropylene triaminepenta-acetic acid; ID, injected dose; MES, (2-(N-morpholino)ethanesulfonic acid hydrate; PI, polydispersity index; ROI, region of interest.

Copyright © 2007 John Wiley & Sons, Ltd.

extracellular agents, distributing non-specifically throughout the plasma and interstitial spaces and being rapidly excreted via the kidneys (7). In the emerging field of cellular and molecular imaging using MRI, more efficient (higher relaxivity) and biospecific CAs are required to deliver as many Gd^{III}-containing species as possible to the cellular targets of interest and therefore attain sufficiently high contrast to obtain their images (8).

At the magnetic field strengths currently used in MRI (0.5–3.0 T, 21.29–127.73 MHz for protons), the aptitude of Gd^{III} chelates to enhance the longitudinal water proton relaxation rate per mmol of CA (relaxivity) is mainly determined by the inner-sphere water-exchange rate (k_{ex}) and the rotational correlation time of the chelate (τ_R) (2–4). The charge of the complex and the steric crowding in the inner coordination sphere have been shown to be the main factors affecting water exchange in Gd^{III} poly(aminocarboxylate) complexes (9,10). Chelators that ensure optimal fast water exchange on the Gd^{III} complex have been developed by inducing steric crowding around the water-binding site, by elongation of the amine backbone or by elongation of a pendant carboxylate arm of the ligand, for both linear (DTPA-type) and macrocyclic (DOTA-type) chelates (11–13), or by replacing a pendant carboxylate by a phosphonate group (14). This facilitates the removal of the water molecule by a dissociative mechanism, accelerating the exchange. Several approaches have been devised to increase τ_R through covalent attachment of Gd^{III} chelates to slowly tumbling macromolecules (2–5), such as carbohydrates (15–17), proteins (18) and dendrimers (19,20). The formation of host–guest non-covalent interactions between Gd^{III} chelates and macromolecules (5,21,22) or β-cyclodextrin oligomers (23) has also been explored. An alternative way to increase τ_R is through self-assembly of amphiphilic Gd^{III} chelates or through inclusion of lipophilic Gd^{III} chelates in liposomes or other lipid-based systems. However, when the water-exchange rate in the Gd^{III} inner sphere is not optimized in these macromolecular agents, their proton relaxivity is still seriously limited.

Lipid-based nanoparticles, such as micelles and liposomes, have been used as colloidal drug carrier vehicles (24–26) and as contrast-enhanced MRI and molecular imaging agents (27,28). Liposomal MRI CAs include, among other types, liposomes entrapping hydrophilic paramagnetic agents in the aqueous lumen or carrying amphiphilic agents on the liposomal surface with the hydrophobic part non-covalently anchored in the lipid bilayer (27,28). In addition to the increased relaxivities, colloidal CAs made up of Gd^{III}-containing supramolecular assemblies can be efficiently taken up by macrophage-rich tissue undergoing endocytosis/phagocytosis (liver and spleen) (29). This provides an efficient way of delivering therapeutic and diagnostic agents to cells with the aid of colloidal-drug-carrier systems. However, the fast sequestration of intravenously injected colloidal-drug carriers from the blood by Kupffer cells (liver/spleen resident macrophages) is a drawback for efficient targeting of drug carriers or diagnostic agents to a specific macrophage population or to non-macrophage sites. As a consequence, there has been increasing interest in the design of colloidal-drug-carrier systems that, by avoiding rapid recognition by Kupffer cells, remain in the blood for long periods. Such carriers have applications in vascular drug delivery and release and site-specific targeting (24). Long-circulating colloidal systems with entrapped radiopharmaceuticals or CAs have been successful in blood-pool imaging (20–32). Micelles prepared from poly(ethylene glycol)–lipid conjugates have been shown to be useful in the delivery of therapeutic or diagnostic agents to areas of myocardial infarction (33).

Micelles may themselves be made up of amphiphilic ions or molecules or can originate separately and act as vehicles to transport poorly soluble compounds (mixed micelles). The effectiveness of micelles as delivery agents depends, among other factors, on their critical micellar concentration (CMC), because, on intravenous injection, micelles are often diluted to less than their CMC.

Several gadolinium-based micelles have been relaxometrically characterized and reported in the literature: linear copolymers of Gd^{III}–DTPA conjugates linked by α,ω-alkyldiamides with a varying number of methylene groups separating the amide function (34,35); Gd^{III}–DTPA-bisamide-$(CH_2)_n$ copolymers ($n = 6$, 10 or 12) (36); Gd^{III}–DOTA derivatives bearing alkyl or monoamide-alkyl aliphatic side chains (C_{10}–C_{18}) (37,38); Gd^{III} chelates of 1,4,7-tris(carboxymethyl)-10-(2-hydroxylalkyl)-1,4,7,10-tetra-azacyclododecane ligands of varying alkyl chain length (39); Gd^{III} chelates of C_8-DOTP and C_{11}-DOTP, two fatty acid analogues of DOTP [1,4,7,10-tetra-azacyclododecane-1,4,7,10-tetrakis(methylenephosphinate)] (40,41); Gd^{III}–3,6,9,15-tetra-azabicyclo[9.3.1]pentadeca-1(15),11,13-triene-3,6,9-triacetate (42); gadofluorine 8 with a Ln^{III}–DO3A monoamide hydrophilic head (Ln = Gd or Y) (43).

The formulation for the preparation of stable mixed micelles based on gadolinium chelates usually includes an amphiphilic Gd^{III} chelate, phospholipid(s) and a surfactant. These micelles should meet the criteria of high contrast efficiency (high relaxivity), small particle size, high loading, good stability and easy production. Several mixed systems have been relaxometrically and/or pharmacologically studied: mixed micelles based on Gd^{III}–DTPA derivatives (44); Gd^{III}–HHD-DO3A-cholesterol (HHD = hydroxyhexadecyl) (45,46); mixed micelles of the Gd^{III}–DTPA–cholesterol conjugate (47); Gd^{III}–DTPA monoamide and bisamide derivatives with alkyl chains (C_{12}, C_{14}, C_{16} or C_{18}) (48,49). Target-specific mixed micelles based on Gd^{III}–C_{18}DTPAGlu/C_{18}CCK8 have also been reported; their effectiveness is due to the presence of the bioactive peptide CCK8, which acts as targeting vector for cholecystokinin (CCK) receptors localized in the cell membrane, which are overexpressed in many tumors (50).

Copyright © 2007 John Wiley & Sons, Ltd.

DOI: 10.1002/nbm

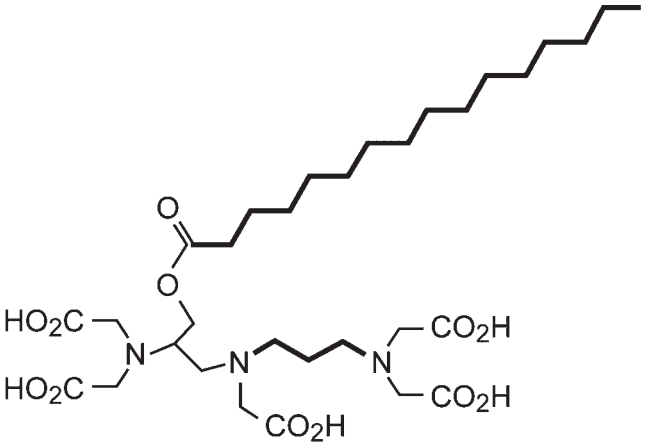

Figure 1. Structure of the metal chelator, H_5EPTPA. The relevant structural features (highlighted) are: substitution of an ethylenediamine bridge by a propylenediamine bridge resulting in stereochemical compression around the water-binding site in the Gd^{3+} complex, and a pendant hydroxymethyl-linked palmitic acid ester moiety rendering the molecule amphiphilic.

We have previously reported the synthesis and characterization of the Gd^{III} complex of the chelator, $H_5EPTPAC_{16}$ [(hydroxymethylhexadecanoyl ester) ethylenepropylene triaminepenta-acetic acid] (Fig. 1) (51). This chelate displays an increased water-exchange rate (k_{ex}) resulting from steric compression around the water-binding site. The attachment of a palmitic ester unit to the ethylenediamine bridge yields an amphiphilic conjugate which forms supramolecular aggregates, possibly micelles, in aqueous solution, with a calculated CMC of 0.34 mM at 25°C (51). A global analysis of the variable-temperature, multiple-field ^{17}O NMR, electron paramagnetic resonance and ^1H NMR dispersion data allowed determination of the parameters governing the relaxivity of $[Gd(EPTPAC_{16})(H_2O)]^{2-}$. The micelles formed in aqueous solution showed considerable internal flexibility, leading to a limited increase in proton relaxivity (51).

In the present work, we studied how the self-assembly of the amphiphilic monomer metal chelates into supramolecular aggregates dramatically influences their *in vivo* behavior and determines their performance as potential imaging agents. We also report the evaluation of the $[^{153}Sm]^{3+}$-labeled compound in Wistar rats through pharmacokinetic studies involving *in vivo* dynamic γ-scintigraphy and biodistribution. The effects of concentration and preparation method (with and without sonication) of the radiotracer $\{[^{153}Sm](EPTPAC_{16})(H_2O)\}^{2-}$ solution on its biodistribution were correlated with the size distribution of the aggregates, determined by dynamic light scattering (DLS). The influence of sonication on $[Ln(EPTPAC_{16})(H_2O)]^{2-}$ in water was monitored by NMR and relaxometry. An *in vivo* MRI study of the contrast effects and pharmacokinetics of the micellar $[Gd(EPTPAC_{16})(H_2O)]^{2-}$ complex in Wistar rats is also reported and compared with a typical commercial, low-molecular-mass CA, GdDTPA (Magnevist®).

EXPERIMENTAL

$H_5EPTPAC_{16}$ was synthesized as described previously (51).

Preparation of Ln^{III}–EPTPA complexes

The general procedure was dissolution of $H_5EPTPAC_{16}$ in distilled water and addition of a molar equivalent of $LnCl_3$ solution (Ln = Eu, Gd). The pH was adjusted to 5.5 with aqueous KOH (0.1 M). The solution was stirred at room temperature for 1 h and then adjusted to pH 7.0 with aqueous KOH (0.1 M). The solution was concentrated at reduced pressure giving rise to a white solid.

For the DLS experiments, 0.2 mM and 2 mM solutions were prepared by dissolving the corresponding $[Gd(EPTPAC_{16})(H_2O)]^{2-}$ complex in 150 mM MES [2-(*N*-morpholino)ethanesulfonic acid hydrate, 99.5%] buffer, pH 6.4. Samples were sonicated using a Bandelin Sonorex RK 106S sonicator (P = 200 W, υ = 35 MHz). Aqueous solutions of $[Gd(EPTPAC_{16})(H_2O)]^{2-}$ were prepared for the relaxometric experiments, whereas the NMR experiments used D_2O solutions of $[Eu(EPTPAC_{16})(H_2O)]^{2-}$.

NMR measurements

^1H NMR spectra were recorded in D_2O (99.99% ^2H) on Varian Unity Plus 300 and Unity 500 NMR spectrometers, operating at 299.938 MHz and 499.80 MHz, respectively. Chemical shifts (δ) are given in ppm relative to TSP as internal reference (^1H, δ 0.0).

Relaxometric measurements

Water ^1H relaxivity measurements were performed on a Bruker Minispec mq60 (60 MHz) at 25°C and 37°C. The temperature was measured by a substitution technique. Longitudinal relaxation rates were measured at four different concentrations, two below (0.1 and 0.2 mM) and two above (2.0 and 4.0 mM) the CMC before and after 2, 4 and 20 min of sonication.

DLS measurements

These were performed on a Coulter® N4 Plus Submicron Particle Sizer. The N4 Plus contains a 10 mW He–Ne

Copyright © 2007 John Wiley & Sons, Ltd.

DOI: 10.1002/nbm

laser which emits monochromatic polarized light with a wavelength of 632.8 nm. The electric field polarization is perpendicular to the plane formed by the incident and detected rays (vertical polarization). The particle size is calculated from the measurement of the sample diffusion coefficient by photon correlation spectroscopy. The N4 Plus is controlled by PC-based software which operates in the Microsoft Windows environment. Before data acquisition, the sample was allowed to equilibrate for 2 min. All the measurements were performed at an angle of 90° and at 20°C. The data acquired were analysed by unimodal analysis, which yields the mean intensity-weighted particle size and standard deviation. The mean intensity-weighted particle size was determined for each solution concentration over time, without and with 2 min of sonication of the solution. Multimodal DLS analysis was performed with a Zetasizer Nano ZS instrument (Malvern Instruments Ltd, Malvern, UK) equipped with a 4 mW He–Ne laser at 633 nm with backscattering detection at 173°.

Reagents for γ imaging and biodistribution studies

$^{153}SmCl_3$ was produced at the Instituto Tecnológico e Nuclear, Lisbon, Portugal by Dr Maria dos Anjos Neves, with a specific radioactivity of >5 GBq/mg. For this purpose, $^{153}Sm_2O_3$ was prepared from a 98% ^{152}Sm-enriched Sm_2O_3 target, sealed into a quartz vial and welded into an aluminum can, by neutron irradiation using a thermal flux of 2.3×10^{13} n/cm$^2 \cdot$ s. After irradiation, the sample was opened, dissolved in 1 M HCl, and the final $^{153}SmCl_3$ solution was brought to a stock concentration of 1.9×10^{-3} M.

Radiotracer preparation

Stock solutions of $H_5EPTPAC_{16}$ were prepared in 150 mM MES buffer, pH 6.4, and mixed with $^{153}SmCl_3$. The solutions were left stirring at room temperature for 1 h. Solutions with different concentrations of the radiotracer, 0.2 mM (below CMC) and 2 mM (above CMC) [CMC = 0.34 mM, determined by relaxometry (51)], were prepared for biodistribution and γ imaging experiments. The solution of 2 mM concentration of radiotracer was prepared by adding to a 0.2 mM solution of the $\{[^{153}Sm](EPTPAC_{16})(H_2O)\}^{2-}$ radiotracer the appropriate amount of non-radioactive $\{[^{152}Sm](EPTPAC_{16})(H_2O)\}^{2-}$ complex.

In vivo γ imaging

A γ camera–computer system (GE 400 GenieAcq; General Electric, Milwaukee, WI, USA) was used for acquisition and preprocessing. Data processing and display were performed on a PC using homemade software developed for the IDL 5.2 computer tool. A well counter (DPC-gamma C_{12}, Los Angeles, CA, USA) with a Compaq DeskPro compatible computer was used for radioactivity counting in the biodistribution studies.

γ images and biological distribution of $[^{153}Sm]^{3+}$ complexes were determined using 200–250 g Wistar rats. All animal studies were carried out in compliance with procedures approved by the appropriate institutional review committees. Conscious rats were allowed free access to food and water *ad libitum*. Groups of four animals (one group for each concentration of the radiotracer with and without sonication) were anesthetized with 50 mg/ml ketamine/2.5% chlorpromazine (10:3, v/v) and injected into the femoral vein with ~200 μCi of the $[^{153}Sm]^{3+}$ complex immediately after the solution had been prepared. Two different injected dose concentrations were studied (0.2 mM and 2 mM) as well as the effect of 2 min of sonication on the γ scintigraphic image. The animals were then positioned in dorsal decubitus over the detector. Image acquisition was initiated immediately before radiotracer injection. Sequences of 180 images (of 10 s each) were acquired to 64 × 64 matrices. In addition, static data were acquired 24 h after the radiotracer injection.

Images were subsequently processed using an IDL-based program (Interactive Data Language, Research Systems, Boulder, CO, USA). For analysis of the transport of radiotracer over time, three regions of interest (ROIs) were drawn on the image files, corresponding to the thorax, liver and left kidney. From these regions, time–radioactivity curves were obtained.

Biodistribution studies

Groups of four animals were injected in the tail vein with ~100 μCi of the $[^{153}Sm]^{3+}$ tracer (at the concentrations and conditions stated in the scintigraphic imaging section) and killed 1 h later. The major organs were excised and weighed, and tissue radioactivity was measured in a γ well counter. Similar biodistribution studies were also performed with the animals referred to in the previous section killed at 24 h.

MRI

Sample formulation/preparation of $[Gd(EPTPAC_{16})(H_2O)]^{2-}$ for MRI. The ligand, $H_5EPTPAC_{16}$ (147.4 mg; 0.218 mmol), was dissolved in distilled water. To this solution was added dropwise an aqueous solution of $Gd(NO_3)_3.6H_2O$ (90.0 mg; 0.199 mmol). The pH was kept at 5.5–6.0 by the addition of NaOH (aqueous solution, 0.1 M). The reaction mixture was left stirring for

Copyright © 2007 John Wiley & Sons, Ltd.

DOI: 10.1002/nbm

1 h. The solution was adjusted to pH 7.0 with NaOH (aqueous solution, 0.1 M), filtered (Filtropur S filters, 0.2 μm), and concentrated under reduced pressure. The absence of free metal was confirmed by the xylenol orange test.

To remove the salts ($NaNO_3$) produced during the synthesis of the $[Gd(EPTPAC_{16})(H_2O)]^{2-}$ complex, a sample was purified by silica-gel 100 C_8 reverse-phase chromatography with gradient elution, 100% water → 100% ethanol. The relevant fractions, identified by reverse-phase C_{18} thin-layer chromatography and conductivity measurement, were pooled, filtered (Filtropur S filters, 0.2 μm), and concentrated under reduced pressure to give the salt-free complex, probably $[Gd(EPTPAC_{16})(H_2O)]Na/K_2$, as a vitreous solid.

***In vivo* MRI studies.** The experimental protocols performed were approved by the appropriate institutional review committees and followed the guidelines of their responsible governmental agency. The MRI experiments were all performed on a Bruker Pharmascan platform (Bruker Medical Gmbh, Ettlingen, Germany) using a 7.0 T horizontal-bore superconducting magnet, equipped with a ^{1}H-selective 60 mm birdcage resonator and a Bruker gradient insert with 90 mm diameter (maximum intensity 300 mT/m). Data were acquired using a Hewlett-Packard console running Paravision software (Bruker Medical) in a Linux environment.

All MRI examinations were carried out on male Wistar rats (n = 4, 250–260 g body weight) anesthetized initially by inhalation in an induction box with O_2 (1 liter/min) containing 3% isoflurane, and maintained during the experiment using a mask and 1–2% isoflurane in O_2. Animals were taped down into a holder to minimize breathing-related motion, and then placed in a heated probe, which kept the core body temperature at ~37°C, monitored by a rectal probe. The physiological state of the animal was monitored throughout the experiment with a Biotrig physiological monitor (Bruker Medical), using the respiratory rate and body temperature. Solutions of $[Gd(EPTPAC_{16})(H_2O)]^{2-}$ and $[Gd(DTPA)(H_2O)]^{2-}$ (Magnevist®; Schering, Berlin, Germany; 100 mM) were prepared in distilled water, and the pH was adjusted to 7.2. The solutions were injected into the catheterized tail vein as a bolus of 200 μL in 20 s (0.2 mmol Gd/kg body weight) using an infusion pump (Panlab, Barcelona, Spain).

T_1-weighted spin-echo anatomical images (TR = 200 ms; TE = 11.7 ms; field of view = 6 × 6 cm; acquisition matrix = 256 × 256; number of averages = 2; slice thickness = 2 mm; two packages of four slices each, centered on the liver and on the kidneys) were acquired in axial orientation. Baseline images were acquired before the administration of our CA, $[Gd(EPTPAC_{16})(H_2O)]^{2-}$. After injection, regional CA uptake was assessed by acquiring sequential images for 1 h (50 images).

MRI data processing. Data were analyzed with software written in-house using IDL. With the aim of comparing the pharmacokinetics obtained from different animals, the data were normalized by calculating the relative enhancement (RE):

$$RE = \frac{(I - I_0)}{I_0} \times 100$$

where I is the signal intensity at any given time after CA injection, and I_0 is the intensity before injection. Pharmacokinetics were analyzed by calculating the average enhancements within different ROIs in each one of the following regions: liver, kidney medulla, kidney cortex, vena cava and muscle.

RESULTS AND DISCUSSION

DLS studies

The effects of concentration and sonication of aqueous $[Gd(EPTPAC_{16})(H_2O)]^{2-}$ solutions on the average particle size and polydispersity index (PI) were studied by DLS at 20°C (Fig. 2). We assumed that the CMC does not change between 25°C (51) and 20°C, as observed for $[Gd(DOTAC_{14})(H_2O)]$ between 5°C and 25°C (38). For $[Gd(EPTPAC_{16})(H_2O)]^{2-}$ concentrations (0.2 mM) below the CMC and without sonication, the mean intensity-weighted particle size was above the working range of the instrument (<3000 nm). After 2 min of sonication, it decreased to ~500 nm, and a heterogeneous population of aggregates was present (PI ~1.0). The duration of the sonication, 2 or 4 min, did not substantially affect either the mean intensity-weighted particle size or the PI (not shown). The aggregates formed on sonication

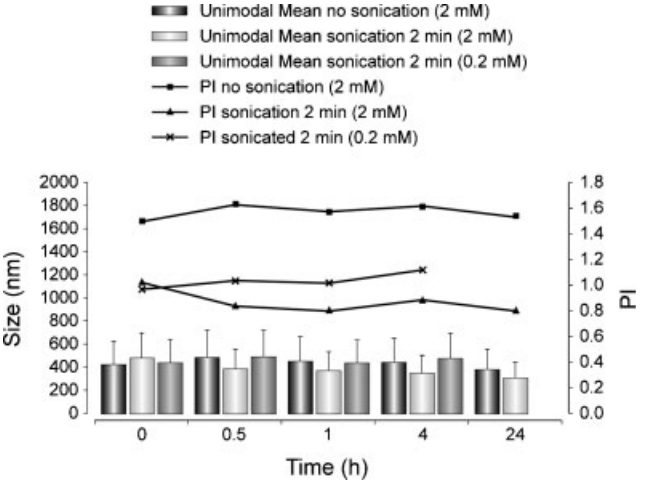

Figure 2. DLS studies on the effect of concentration and sonication of the $[Gd(EPTPAC_{16})(H_2O)]^{2-}$ solution on the average particle size (mean ± SD) and population distribution, as measured by PI.

Copyright © 2007 John Wiley & Sons, Ltd.

DOI: 10.1002/nbm

remained stable for at least 4 h with regard to size and polydispersity (Fig. 2). For $[Gd(EPTPAC_{16})(H_2O)]^{2-}$ solutions of concentration 2 mM (above the CMC), the mean intensity-weighted particle size (~450 nm) was the same before and after 2 min of sonication. However, sonication reduced the heterogeneity of the aggregates, as indicated by a decrease in PI from ~1.5 to ~1.0. Furthermore, both the mean intensity-weighted particle size and the PI decreased over time, reaching values of ~300 nm and ~0.8, respectively, after 24 h (Fig. 2).

For all concentrations studied, both below and above the CMC, with and without sonication, a DLS multimodal analysis (data not shown) revealed populations of at least two particle sizes: small particles (diameter <10 nm), and very large particles (diameter >100 nm) of variable size. The existence of large particles for concentrations below the CMC suggests premicellar aggregation. This is in agreement with a recent study of micelle formation caused by surfactants in the presence of a reporting dye using fluorescence correlation spectroscopy that demonstrated the formation of aggregates in the concentration range (0.3–1.0) × CMC, in increasing number when approaching the CMC (52). Premicellar aggregation has been shown to be responsible for anomalies of various physical parameters (53,54). The large aggregates probably represent only a very small population below the CMC. Indeed, the value of the calculated mean intensity-weighted particle size can be dominated by a very small population of large particles with high scattering intensity. This is also in accordance with the fact that, using relaxometry, we did not observe any slowly rotating large particles below 0.34 mM (CMC determined by relaxivity measurements) (51). Even if below the CMC the large aggregates represent a significant proportion of the population of particles, they can be extremely flexible, which implies that the proton relaxivities will not be much increased with regard to the monomer state.

In conclusion, at a concentration just below the CMC (0.2 mM in our case), the aggregate morphology and dynamics can be quite complicated. DLS data at concentrations lower than 0.2 mM would have certainly been more representative of the 'non-aggregated' state.

Effect of sonication on the NMR spectra and water relaxivity of $[Ln(EPTPAC_{16})(H_2O)]^{2-}$ solutions

The ^{1}H NMR spectrum of a 10 mM D_2O solution of $[Eu(EPTPAC_{16})(H_2O)]^{2-}$ contains a large number of high-frequency (e.g. +25.42, +17.27, +14.93, +13.23, +12.33, +11.67, +7.96 ppm) and low-frequency (−1.58, −2.43, −3.04, −3.55, −4.04, −7.45, −10.45, −10.64 ppm) paramagnetically shifted resonances. This spectrum (available online as Fig. 1S in Supplementary Material) is not affected by sonication periods of up to 20 min, or after a subsequent period of 1 day, showing that sonication does not affect the stability and structure of the complex.

The effect of increasing sonication periods up to 20 min on the 60 MHz water ^{1}H longitudinal relaxivity (r_1) of $[Gd(EPTPAC_{16})(H_2O)]^{2-}$ solutions was studied at different concentrations and temperatures (25°C and 37°C), as shown in Table 1 for 0.2 mM and 2.0 mM concentrations. At the measurement frequency of 60 MHz (close to the maximum of the NMR dispersion curves of the complex in the micellar form), r_1 is mainly determined by the rotational dynamics of the chelate (51). Hence the variation in r_1 reflects the changes in the rotational dynamics of the micellar aggregates. As the CMC is expected to increase by ~10% between 25°C and 37°C (38), at 37°C 0.2 mM is still below the CMC (51). Above the CMC and at any of the temperatures, sonication had no significant influence on r_1. This indicates that sonication does not affect the average rotational dynamics of the chelate in the micellar aggregates, as reflected by the r_1 values [more precisely, r_1 is determined by the global (τ_g) and segmental (τ_l) rotational correlation times of the aggregates (51)]. This is in qualitative agreement with the DLS observation that the mean intensity-weighted particle size was not affected by sonication at concentrations above the CMC. Below the CMC, r_1 values, which are about half the values above the CMC, increased with sonication at both temperatures. At 25°C, this increase became larger with sonication time, from 9% (2–4 min) to 14% (20 min). At 37°C, the r_1 increase was only significant (9%) for 20 min of sonication. As

Table 1. Effect of sonication on the 60 MHz water ^{1}H longitudinal relaxivity (r_1) of $[Gd(EPTPAC_{16})(H_2O)]^{2-}$ solutions at different temperatures and concentrations below and above the CMC. The results are mean ± SD from three measurements

	r_1 ($mM^{-1}s^{-1}$)			
	25°C		37°C	
	0.2 mM	2.0 mM	0.2 mM	2.0 mM
No sonication	9.94 ± 0.01	20.55 ± 0.01	6.46 ± 0.01	15.63 ± 0.01
2 min sonication	10.94 ± 0.04	20.61 ± 0.01	6.53 ± 0.02	15.63 ± 0.01
4 min sonication	10.96 ± 0.02	20.62 ± 0.01	6.53 ± 0.02	15.63 ± 0.01
20 min sonication	11.66 ± 0.01	20.63 ± 0.01	7.06 ± 0.04	15.63 ± 0.01

Copyright © 2007 John Wiley & Sons, Ltd.

DOI: 10.1002/nbm

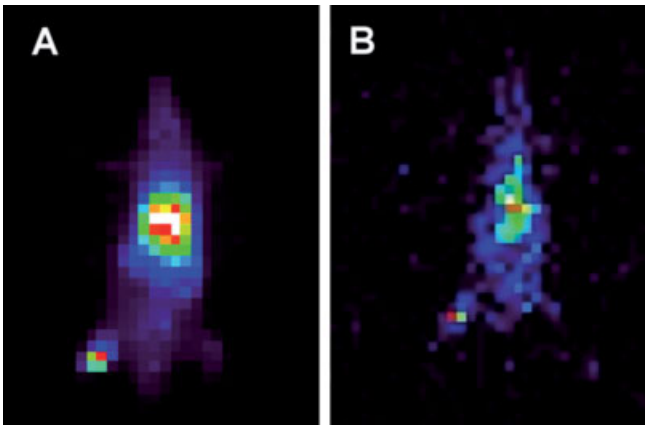

Figure 3. Scintigraphic image at 30 min of a Wistar rat injected with a 0.2 mM solution of $\{[^{153}Sm](EPTPAC_{16})(H_2O)\}^{2-}$ (A) without sonication and (B) after 2 min of sonication.

discussed above, the situation at concentrations just below the CMC is rather complex with regard to the formation of preaggregates. Moreover, these structures are probably very fluxional and may change on sonication. These factors may explain why the significant decrease in mean intensity-weighted particle size detected by DLS was not observed in the relaxivities. Concentrations significantly lower than 0.2 mM would be much more useful for examining the non-aggregated state.

Studies of $[^{153}Sm]^{3+}$-labeled $EPTPAC_{16}$ complex

***In vivo* γ-imaging and biodistribution.** Scintigraphic images of Wistar rats were obtained as a function of time after injection of an aqueous solution of 0.2 mM $\{[^{153}Sm](EPTPAC_{16})(H_2O)\}^{2-}$ tracer (below CMC). Fig. 3 compares the images obtained 30 min after injection of the tracer solution without and after 2 min of sonication. Without previous sonication, there is a marked high uptake/retention of the tracer in the thorax. Further experiments (dynamic acquisition and biodistribution; see below) revealed that the uptake of the radiotracer occurred predominantly in the lungs. In sharp contrast, 2 min of sonication of the 0.2 mM radiotracer solution resulted in high liver uptake and virtually no uptake in the lungs, as demonstrated by dynamic acquisition and biodistribution (see below).

Time–radioactivity curves for the 0.2 mM $\{[^{153}Sm](EPTPAC_{16})(H_2O)\}^{2-}$ radiotracer without and after 2 min of sonication were obtained in dynamic acquisition experiments (Fig. 4). The curves were smoothed and normalized in relation to the maximum radioactivity obtained. The radioactivity of the 0.2 mM radiotracer without sonication increased sharply in the thorax immediately after the injection, possibly corresponding to lung uptake/retention of the radiolabeled complex, and decayed very slowly over the duration of the experiment. After 30 min, the radioactivity remaining in the thorax/

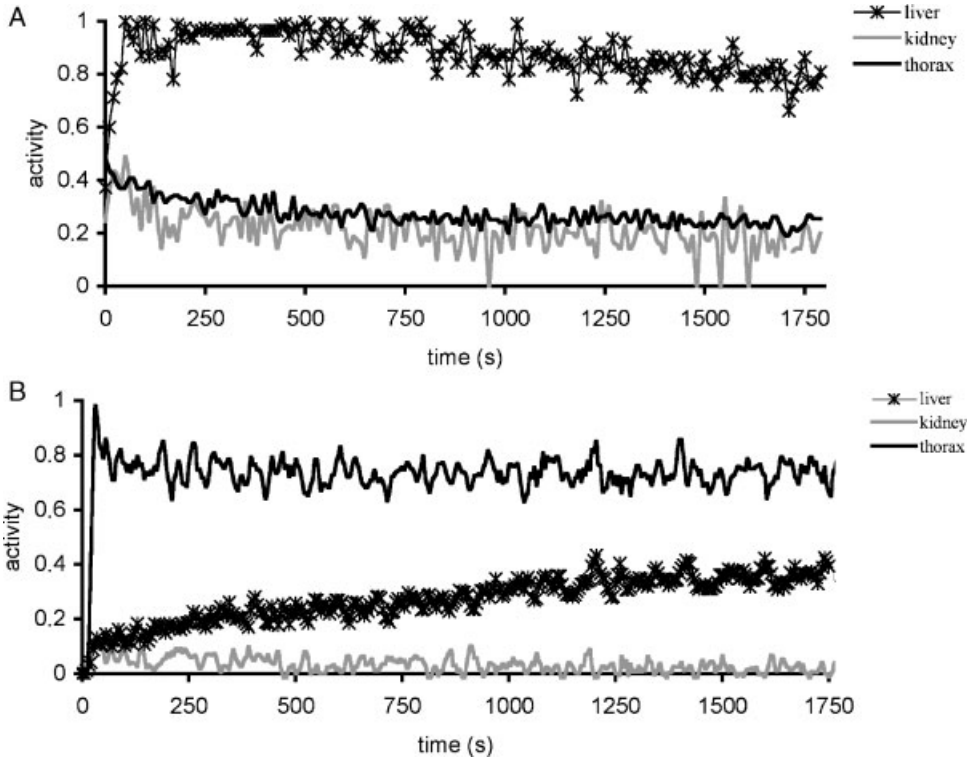

Figure 4. Time–radioactivity curves at various ROIs (liver, kidney and thorax) in Wistar rats after the injection of a 0.2 mM solution of the radiotracer $\{[^{153}Sm](EPTPAC_{16})(H_2O)\}^{2-}$ after 2 min of sonication (A) and without sonication (B).

Copyright © 2007 John Wiley & Sons, Ltd.

DOI: 10.1002/nbm

lungs was still ~80% of the maximum obtained for this region. In contrast, the radioactivity in the liver increased smoothly over the duration of the experiment, and after 30 min it was approximately half of that remaining in the lungs. There was virtually no uptake of radioactivity by the kidney, consistent with the lipophilic nature of the radiotracer and its putative hepatobiliary excretion pathway. Sonication of the radiotracer solution before injection had a dramatic effect on the dynamic acquisition curves. The radioactivity in the liver increased sharply after the injection and reached its highest value after ~1 min, which can be ascribed to the liver first-pass uptake of the radiotracer. From there on, the radioactivity in the liver decayed slowly and smoothly, remaining at ~80% after 30 min. The radioactivity in the thorax and kidneys increased immediately after the injection, and then decayed constantly during the experiment. After 30 min, the radioactivity was located mainly in the liver.

The effect of sonication on the biodistribution pattern of $\{[^{153}Sm](EPTPAC_{16})(H_2O)\}^{2-}$ in Wistar rats at 1 and 24 h after injection was studied for concentrations of the radiotracer below (0.2 mM) and above (2 mM) the CMC. Fig. 5 and Table 2 show representative data as a percentage of injected dose per gram of tissue (%ID/g).

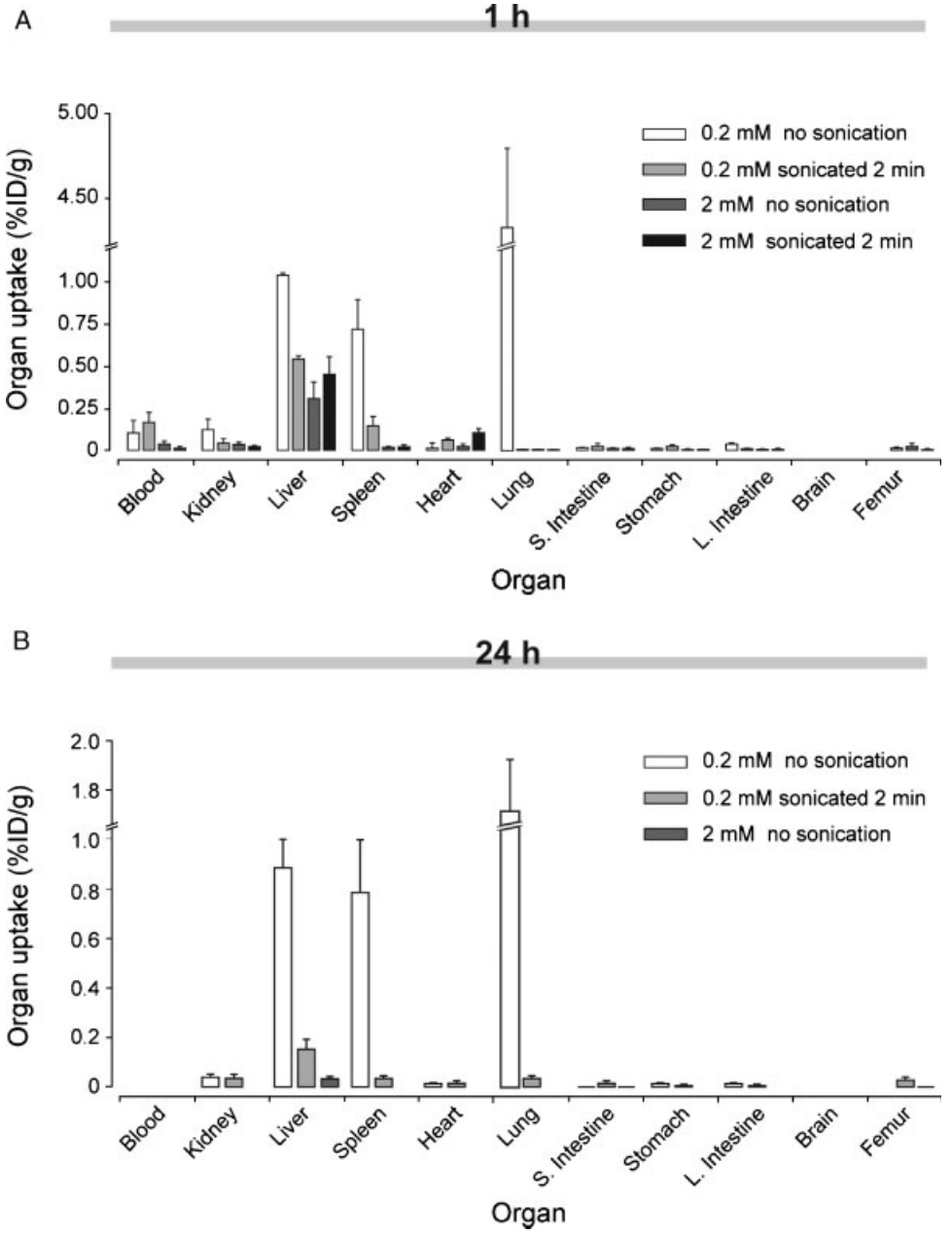

Figure 5. Biodistribution in Wistar rats (percentage of the injected dose/g of organ) of $\{[^{153}Sm](EPTPAC_{16})(H_2O)\}^{2-}$ at 1 h (A) and 24 h (B) after the injection for radiotracer concentrations of 0.2 and 2 mM, with and without sonication. S. Intestine, small intestine; L. Intestine, large intestine. Values are mean ± SD.

Copyright © 2007 John Wiley & Sons, Ltd.

DOI: 10.1002/nbm

Table 2. Biodistribution of $\{[^{153}Sm](EPTPAC_{16})(H_2O)\}^{2-}$ at 1 h and 24 h after injection in Wistar rats for radiotracer concentrations of 0.2 and 2 mM without sonication and after sonication for 2 min. Results are mean ± SD from groups of four animals

	%ID/g (1 h)				%ID/g (24 h)		
	0.2 mM		2 mM		0.2 mM		2 mM
Organ	No sonication	Sonicated	No sonication	Sonicated	No sonication	Sonicated	No sonication
Blood	0.11 ± 0.07	0.17 ± 0.06	0.042 ± 0.016	0.02 ± 0.01	0.0010 ± 0.0002	0.0016 ± 0.0008	0.00007 ± 0.00003
Kidney	0.13 ± 0.06	0.05 ± 0.02	0.04 ± 0.01	0.03 ± 0.01	0.04 ± 0.01	0.03 ± 0.02	0.004 ± 0.001
Liver	1.04 ± 0.01	0.55 ± 0.02	0.31 ± 0.10	0.46 ± 0.10	0.86 ± 0.11	0.15 ± 0.04	0.03 ± 0.01
Spleen	0.72 ± 0.18	0.15 ± 0.06	0.02 ± 0.01	0.02 ± 0.01	0.76 ± 0.21	0.03 ± 0.01	0.003 ± 0.001
Heart	0.02 ± 0.03	0.06 ± 0.01	0.03 ± 0.01	0.11 ± 0.02	0.012 ± 0.003	0.01 ± 0.01	0.0015 ± 0.0007
Lung	4.32 ± 0.47	0.0090 ± 0.0003	0.0075 ± 0.0002	0.007 ± 0.002	1.68 ± 0.20	0.008 ± 0.005	0.0005 ± 0.0002
Femur	—	0.018 ± 0.003	0.03 ± 0.02	0.008 ± 0.002	—	0.03 ± 0.01	0.003 ± 0.001

Above the CMC, the sonication seems not to have had a significant effect on the biodistribution pattern. The radioactivity was located mainly in the liver, with very low %ID/g found in the blood, kidney, spleen and heart. These results are consistent with the DLS studies, which showed that, for concentrations of the radiotracer above the CMC, it exists as ''small'' particles (mean intensity-weighted particle size ~450 nm), which are efficiently taken up by the liver-resident macrophages (Kupffer cells). Moreover, the DLS studies showed that, above the CMC, sonication had no significant effect on the size of aggregates and therefore on the biodistribution pattern.

Below the CMC and without sonication, there was a very high uptake and retention of the radiotracer by the lungs, and significant radioactivity was taken up by the liver (even higher than its value above the CMC) and spleen, and to a much lesser extent by the kidney and blood. These results are consistent with the DLS studies, which showed the existence of very large micellar aggregates in solution (diameter >3000 nm) in these experimental conditions. These large aggregates were efficiently taken up by resident macrophages in lungs, liver and spleen (reticuloendothelial system). The high lung uptake may also be due to entrapment of very large particles in the narrow lung capillaries. In fact, pulmonary

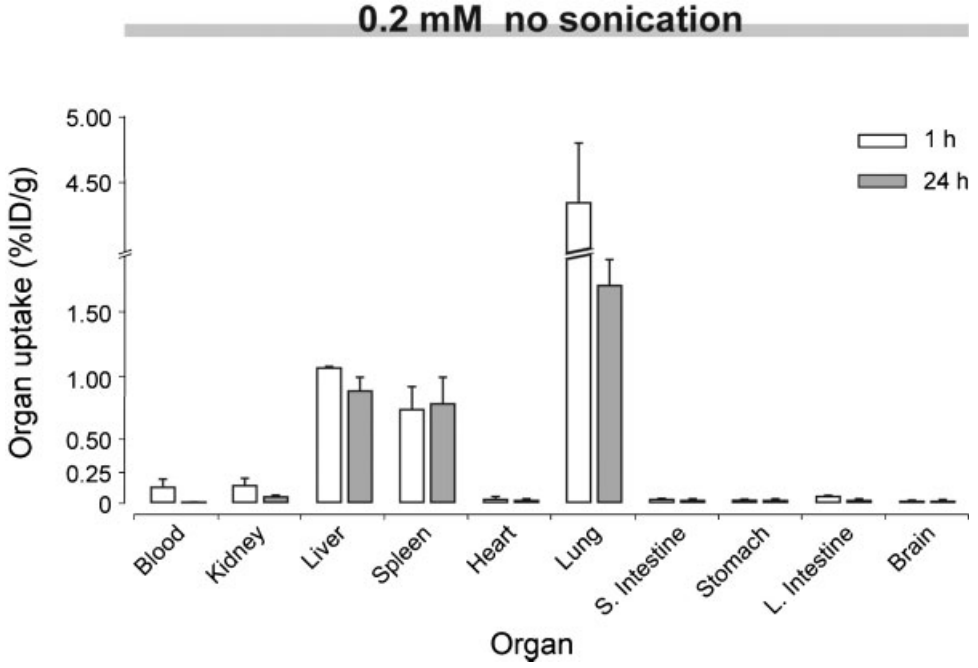

Figure 6. Comparison of the biodistribution in Wistar rats (percentage of the injected dose/g of organ) of $\{[^{153}Sm](EPTPAC_{16})(H_2O)\}^{2-}$ at 1 h and 24 h after injection for a radiotracer concentration of 0.2 mM without sonication. S. Intestine, small intestine; L. Intestine, large intestine. Values are mean ± SD.

Copyright © 2007 John Wiley & Sons, Ltd.

DOI: 10.1002/nbm

precapillaries are only 8 μm in length and 10–15 μm in diameter. Thus, particles with diameters exceeding 10 μm cannot pass through the smallest capillaries and are therefore filtered out of the circulation on arrival at these vessels (55). This is the reason for the use of ^{99m}Tc-labeled macro-aggregated albumin to evaluate lung perfusion (56).

The most striking result of the biodistribution studies is the dramatic effect of sonication on the biodistribution pattern 1 h after the injection at concentrations of the radiotracer below the CMC. After sonication, radioactivity in the lungs virtually disappeared, being mainly taken up by the liver and to a lesser extent by the spleen. This biodistribution pattern is virtually equivalent to that found at radiotracer concentrations above the CMC, the only difference being some uptake by the spleen. These results are again consistent with the DLS studies, which revealed that sonication of the radiotracer solution below the CMC significantly reduced the size of the particles (from a diameter of >3000 nm to a mean intensity-weighted particle size of ~450 nm). It is also striking that, with the 0.2 mM non-sonicated radiotracer (concentration below the CMC), there was still very significant radioactivity in the lungs, liver and spleen after 24 h. In fact, in the 24 h time span, the liver %ID/g decrease in non-sonicated radiotracer was ~90% at 2 mM compared with only ~18% at 0.2 mM. In the same time interval, this value for the 0.2 mM non-sonicated radiotracer was reduced in the lungs by ~40% and increased by ~6% in the spleen. This resulted in a total %ID/g ratio (lung/liver plus spleen) decrease from 2.40 at 1 h to 1.03 at 24 h, because of the large relative mass of the liver. These results suggest that the lungs work as a reservoir of (possibly entrapped) radiotracer, which is slowly released and taken up by the liver and spleen reticuloendothelial system (Fig. 6). For 0.2 mM sonicated radiotracer, the %ID/g reduction in the liver and spleen at 24 h was respectively ~73% and ~80%.

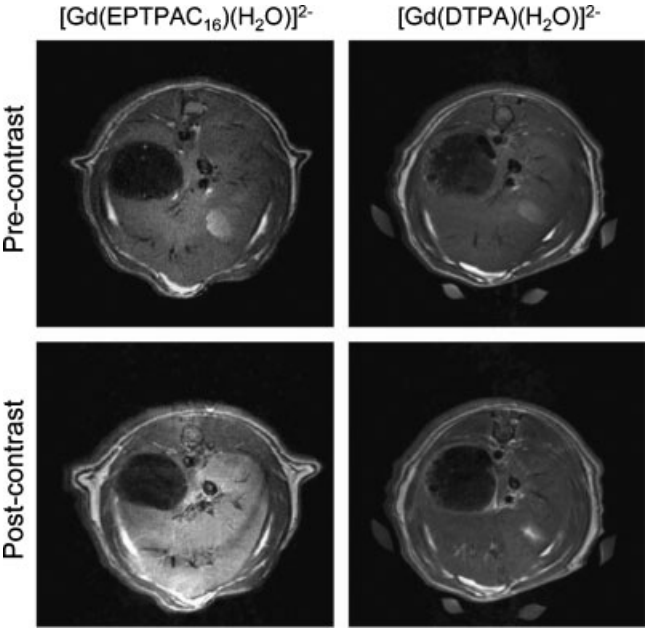

Figure 7. T_1-weighted spin-echo axial MR images of rat liver before (upper panels) and after (lower panels) the injection of 0.2 mmol/kg $[Gd(EPTPAC_{16})(H_2O)]^{2-}$ (left) or $[Gd(DTPA)(H_2O)]^{2-}$ (right).

We have interpreted the biodistribution data for $\{[^{153}Sm](EPTPAC_{16})(H_2O)\}^{2-}$ on the basis of the CMC determined by relaxometry for the corresponding Gd^{3+} complex (51) and correlating the data with the size distribution of the particles as determined by DLS. However, the physical state and fate of the radiotracer once injected is uncertain. On injection, the resulting dilution, which depends on the volume of the blood compartment, may reduce the concentration of the radiotracer to below the CMC, even when injected at concentrations above the CMC. The situation is even

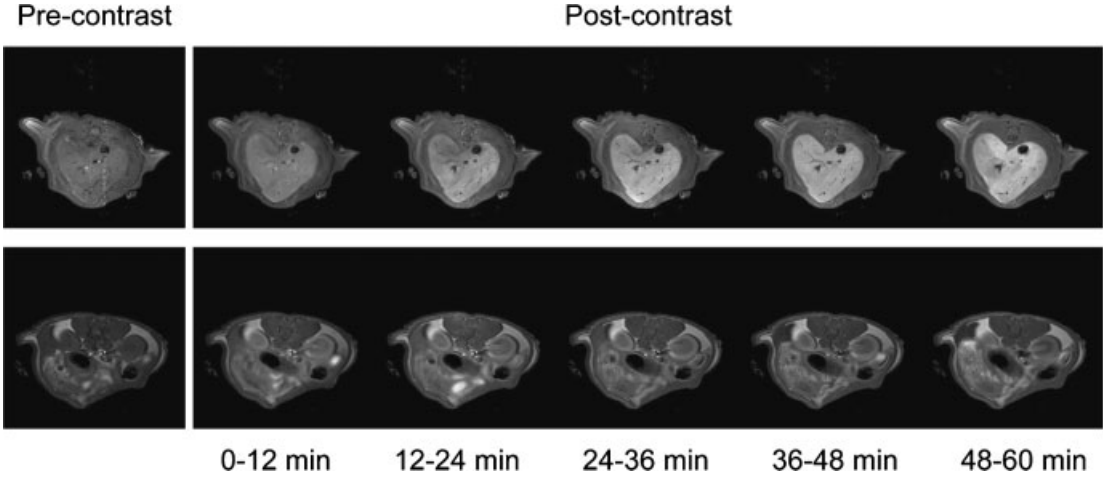

Figure 8. Representative T_1-weighted DCE-MRI series of rat liver (above) and kidney/muscle (below) axial images before and after the injection of $[Gd(EPTPAC_{16})(H_2O)]^{2-}$ (0.2 mmol/kg). Each pre-contrast and post-contrast image corresponds to the average of three time points (~4 min) or 10 time points (12 min), respectively.

Copyright © 2007 John Wiley & Sons, Ltd.

DOI: 10.1002/nbm

more complex when the concentration of the radiotracer is already below the CMC when injected. The non-covalent association of $\{[^{153}Sm](EPTPAC_{16})(H_2O)\}^{2-}$ with plasma lipoproteins through anchorage of the fatty acid chain at their phospholipid monolayer may occur, as shown for the DTPA–bis(steraylamide) complexes of Gd^{3+} and $[^{111}In]^{3+}$ with high-density lipoproteins and low-density lipoproteins (57–59). This would allow their transport and delivery to the liver by receptor-mediated endocytosis, which would modify the tracer biodistribution.

MRI

Effect of the Gd chelate on vital functions. The CA was well tolerated by the mice. Their body temperature remained stable, but respiration rate increased to 120 breaths/min during the first 2–3 min after injection, returning to baseline values within 3 min.

MRI *in vivo*. Series of T_1-weighted spin-echo axial images of the DCE MRI experiments were obtained with the $[Gd(EPTPAC_{16})(H_2O)]^{2-}$ complex (dose 0.2 mmol/kg

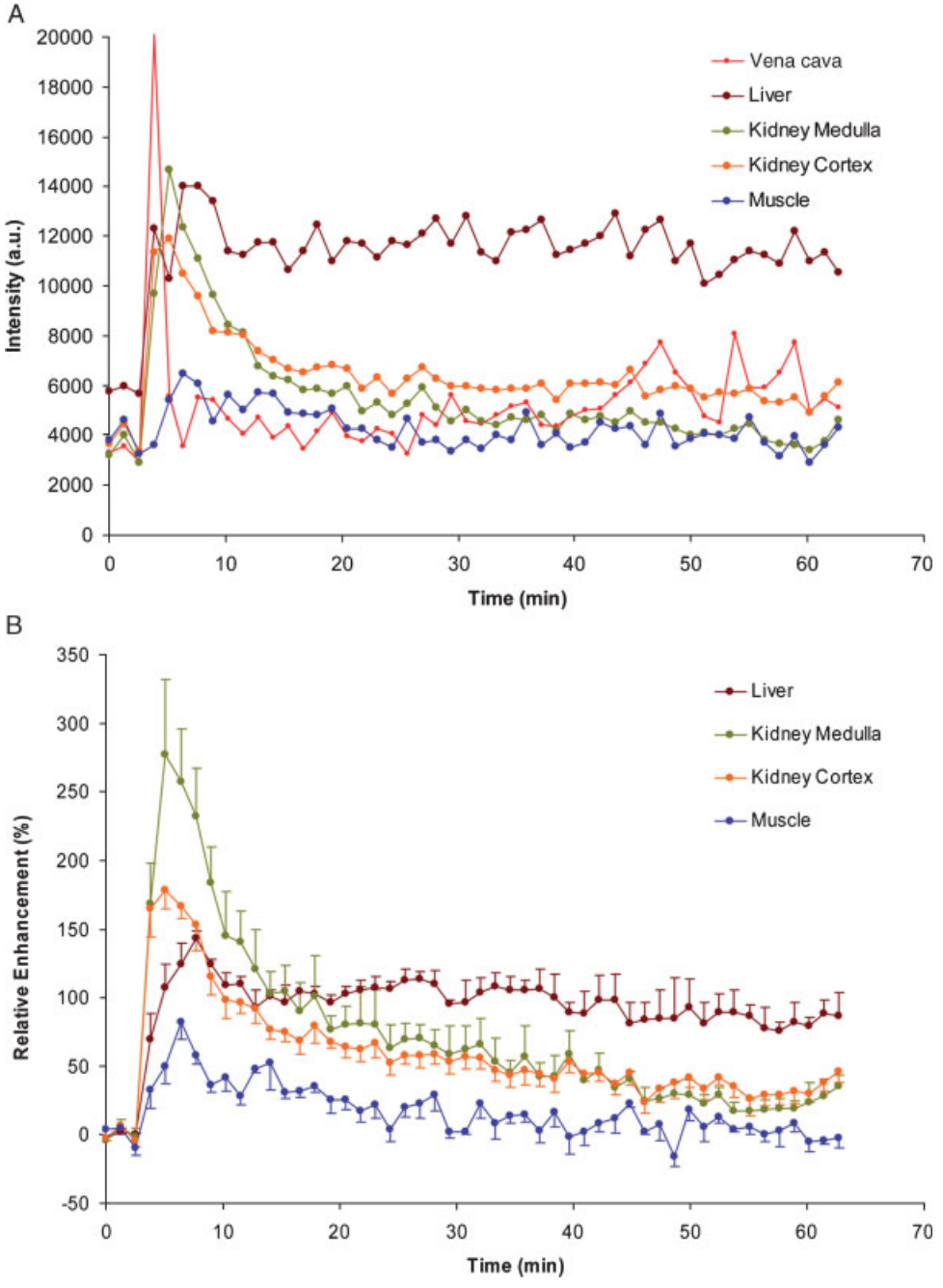

Figure 9. Time course of signal intensity (A) and relative enhancement (B) of several ROIs during DCE-MRI experiments after the injection of $[Gd(EPTPAC_{16})(H_2O)]^{2-}$ (0.2 mmol/kg). (A) Data from an individual animal. (B) Mean ± SE from four animals.

Copyright © 2007 John Wiley & Sons, Ltd.

DOI: 10.1002/nbm

body weight) and $[Gd(DTPA)(H_2O)]^{2-}$ (dose 0.2 mmol/kg body weight). The $[Gd(EPTPAC_{16})(H_2O)]^{2-}$ complex induced a marked increase in the liver, whereas $[Gd(DTPA)(H_2O)]^{2-}$ had no significant effect (Fig. 7).

A representative series of DCE-MRI data is shown in Fig. 8; the images correspond to the average of three (pre-contrast) or 10 (post-contrast) time points. The enhancement in the liver after injection of $[Gd(EPTPAC_{16})(H_2O)]^{2-}$ reached a steady state that was maintained until the end of the experiment. In contrast, the enhancement observed in the kidneys and muscle was transitory. This is better illustrated in Fig. 9A, which shows a quantitative analysis of the same dataset. Each time point corresponds to the average intensity within the ROIs in the different organs. For comparison of the results of all the animals under study, the data were normalized by calculating the mean relative enhancement of each ROI for the four animals studied (Fig. 9B). Maximum enhancement was reached within the first 5 min of the injection in all cases. The initial relative enhancement rose quickly to a maximum that was higher in the kidney medulla (280%) and cortex (175%) than in the liver (145%). However, it rapidly decreased in the kidney to below 90% after 20 min, whereas the enhancement in the liver remained approximately constant as the predominant effect throughout the experiment (105% to 100% between 12 and 60 min). Fig. 9A also shows that the contrast enhancement in the abdominal vena cava was also intensified, although more briefly than in the abdominal aorta with another colloidal agent, GdDTPA–DeA (60).

CONCLUSIONS

We have recently reported on a new amphiphilic Gd^{III} complex, $[Gd(EPTPAC_{16})(H_2O)]^{2-}$, which self-assembles into supramolecular structures, possibly micelles, with a CMC of 0.34 mM as determined by relaxometry and surface tension measurements (51). Although its stability constant could not be determined by potentiometry because of precipitation at acid pH, its stability should be similar to that of $[Gd(EPTPA)(H_2O)]^{2-}$ (the $EPTPACH_2OH$ ligand is not linked by an ester group to the long fatty acid chain; $\log K_{GdL} = 16.7$) (61), as the two ligands have very similar protonation constants (61). This stability is indeed lower than for the parent unsubstituted chelate, $[Gd(EPTPA)(H_2O)]^{2-}$ ($\log K_{GdL} = 18.75$), for the substituted $[Gd(EPTPA\text{-}bz\text{-}NO_2)(H_2O)]^{2-}$ ($\log K_{GdL} = 19.20$) or for $[Gd(DTPA)(H_2O)]^{2-}$ ($\log K_{GdL} = 22.50$) (12). However, *in vivo* dissociation of the $EPTPAC_{16}$ complex does not seem to occur, as no accumulation of radioactive $[^{153}Sm]^{3+}$ is observed in the rat skeleton (see data for femur in Table 2). We also believe that the ester function of the $[Ln(EPTPAC_{16})(H_2O)]^{2-}$ complexes is stable in water during sonication, as this treatment did not cause precipitation of the long-chain fatty acid, had no effect on the ^{1}H-NMR spectrum of $[Eu(EPTPAC_{16})(H_2O)]^{2-}$ {in particular, no new resonances corresponding to the hydrolysis product, $[Eu(EPTPA)(H_2O)]^{2-}$, were observed (61)} nor on the r_1 relaxivity of $[Gd(EPTPAC_{16})(H_2O)]^{2-}$ below and above the CMC, which was quite different from that of $GdEPTPACH_2OH$ (61).

Here we present DLS studies on aqueous $[Gd(EPTPAC_{16})(H_2O)]^{2-}$ solutions which demonstrate the existence of aggregates of different sizes both slightly below and above the CMC. This evidence for premicellar aggregation is in accordance with previously reported data for cationic and anionic surfactants (52). As the CMC is known to depend on the physical method used to determine it, the value determined by relaxometry, corresponding to a discontinuity in the relaxometric behavior of the $[Gd(EPTPAC_{16})(H_2O)]^{2-}$ complex as a function of the concentration, must be taken as a reasonable approximation, close to that obtained by classical surface tension measurements (38).

Slightly below the CMC (0.2 mM), the $[^{153}Sm]^{3+}$-labeled chelate was taken up strongly by macrophage-rich tissues (spleen, liver and lungs), in accordance with the existence in solution of very large particles (as determined by DLS), which are physically trapped in the lungs (which seem to function as a chelate reservoir) and slowly released and taken up by the liver and spleen (as shown by the biodistribution data after 24 h). Above the CMC, the chelate is mainly taken up by the liver, with very little uptake by the spleen and lungs. This is consistent with the presence in solution of smaller particles. Sonication of the 0.2 mM radiotracer solution has a major effect on its biodistribution: it is mainly taken up by the liver, whereas its uptake by the lungs virtually ceases. This is consistent with the reduction in size of the particles after sonication to one similar to that found in the 2 mM solution. This is not reflected in any significant change in internal aggregate flexibility and r_1 relaxivity, as opposed to the effect of rigidification of bilayer structures on r_1 (62).

At the radiotracer concentrations investigated here, there are aggregates in solution with different sizes and structures, in particular at concentrations slightly below the CMC; this is due to the presence of premicellar aggregates. The monomodal DLS analysis performed gives only a simplified view of the very complex population dynamics through the weight-averaged particle size and an index (PI) of population heterogeneity. Furthermore, the effect of the dilution of the metal complex that occurs on injection on the size and type of aggregates formed in the blood is difficult to predict. In addition, the amphiphilic Gd^{III} chelate has the potential to associate with plasma lipoproteins (57–59) by intercalation of the lipophilic chain into their phospholipid monolayers. These facts, taken together, make detailed interpretation of the *in vivo* studies difficult. This work highlights the complexity and subtlety of the *in vivo* behavior of what appears to be a simple system. Nonetheless, the rather simplistic correlation between effect of concentration and preparation (with sonication and without sonication) of

Copyright © 2007 John Wiley & Sons, Ltd.

DOI: 10.1002/nbm

the metal chelator on particle size (determined by DLS) and the biodistribution seems to be significant.

In contrast with liposomal CAs that carry the paramagnetic amphiphilic Gd^{III} chelate in the lipid bilayer, which has been reported in various *in vivo* studies (27,28, 63,64), very few targeted or non-targeted Gd^{III}-based colloidal CAs have been studied beyond the stage of basic physicochemical characterization (29,50,63). The present *in vivo* DCE-MRI evaluation of the micellar $[Gd(EPTPAC_{16})(H_2O)]^{2-}$ compound in Wistar rats shows a persistent hepatic positive-contrast effect in T_1-weighted images, which is qualitatively similar to that of the clinically-established Gd^{III}-based hepatobiliary agents, Gd-EOB-DTPA (65) and Gd-BOPTA [where BOPTA is 4-carboxy-5,8,11-tris(carboxymethyl)-1-phenyl-2-oxa-5, 8,11-triazatridecan-13-oate] (66), although a comparative study was not undertaken. No enhancement effect was seen in the lungs because of the scarcity of mobile protons in this organ, despite the scintigraphic evidence for significant lung retention of the $[^{153}Sm]^{3+}$-labeled chelate at concentrations below the CMC. The possibility of using this type of micellar compound for imaging lung pathologies involving water accumulation, which will depend on the degree of dilution of the imaging agent in the body relative to its CMC, is worth pursuing in future studies.

Acknowledgments

This work was financially supported by the Foundation of Science and Technology (FCT), Portugal (project POCTI/QUI/47005/2002 and Ph.D. grant SFRH/BD/5407/2001 to T.B.R.), Instituto de Investigação Interdisciplinar University of Coimbra, Portugal (grant III/BIO/45/2005), FEDER, the Institute of Health Carlos III, Spain, PI051845 (to M.L.G.M.), and the Spanish Ministry of Education and Science, grants SAF 2004-0391 and NAN2004-09125-C07-03 (to S.C.). We thank Dr Maria dos Anjos Neves, at the Instituto Tecnológico e Nuclear, Lisbon, Portugal for providing $^{153}SmCl_3$. The work was carried out in the framework of the EC COST Actions D18 'Lanthanide chemistry for diagnosis and therapy' and D38 'Metal-Based Systems for Molecular Imaging Applications;, the European-funded EMIL program (LSCH-2004-503569), and the Acção Integrada Luso-Espanhola E-10/04.

REFERENCES

1. Caravan P, Ellison JJ, McMurry TJ, Lauffer RB. Paramagnetic metal complexes as water proton relaxation agents for NMR imaging. *Chem. Rev.* 1999; **99**: 2293–23525.
2. Tóth É, Merbach AE (eds). *The Chemistry of Contrast Agents in Medical Magnetic Resonance Imaging*. Wiley: Chichester, 2001.
3. Tóth É, Helm L, Merbach AE. Relaxivity of MRI contrast agents. *Top. Curr Chem.* 2002; **221**: 61–101.
4. Tóth É, Helm L, Merbach AE. MRI contrast enhancement agents. In *Comprehensive Coordination Chemistry II*, McCleverty JA, Meyer TJ (eds). Publisher: Elsevier Ltd.: Oxford, UK, 2004; **9**: 841–881.
5. Aime S, Botta M, Fasano M, Terreno E. Lanthanide(III) chelates for NMR biomedical applications. *Chem. Soc. Rev.* 1998; **27**: 19–29.
6. Comblin V, Gilsoul D, Hermann M, Humbert V, Jacques V, Mesbari M, Sauvage C, Desreux JF. Designing new MRI contrast agents: a coordination chemistry challenge. *Coord. Chem. Rev.* 1999; **185–186**: 451–470.
7. Gries H. Extracellular MRI contrast agents based on gadolinium. *Top. Curr Chem.* 2002; **221**: 1–24.
8. Aime S, Cabella C, Colombato S, Crich SG, Gianolo E, Maggiori F. Insights into the use of paramagnetic Gd(III) complexes in MR-molecular imaging investigations. *J. Magn. Reson. Imaging* 2002; **16**: 394–406.
9. Tóth É, Burai L, Brücher E, Merbach AE. Tuning water-exchange rates on (carboxymethyl)iminobis(ethylenenitrilo)tetraacetate (DTPA)-type gadolinium(III) complexes. *J. Chem. Soc. Dalton Trans.* 1997; 1587–1594.
10. André JP, Maecke HR, Tóth É, Merbach AE. Synthesis and physicochemical characterization of a novel precursor for covalently bound macromolecular MRI contrast agents. *J. Biol. Inorg. Chem.* 1999; **4**: 341–347.
11. Ruloff R, Tóth É, Tripier R, Handle H, Merbach AE. Accelerating water exchange for Gd(III) chelates by steric compression around the water binding site. *Chem. Commun.* 2002; **22**: 2630–2631.
12. Laus S, Ruloff R, Tóth É, Merbach AE. Gd^{III} complexes with fast water exchange and high thermodynamic stability: potential building blocks for high-relaxivity MRI contrast agents. *Chemistry* 2003; **9**: 3555–3566.
13. Jászberényi Z, Sour A, Tóth É, Benmelouka M, Merbach AE. Fine-tuning water exchange on Gd^{III} poly(amino carboxylates) by modulation of steric crowding. *Dalton Trans.* 2005; 2713–2719.
14. Kotek J, Lebdůková P, Hermann P, van der Elst L, Muller RN, Geraldes CFGC, Maschmeyer T, Lukeš I, Peters JA. Lanthanide(III) complexes of novel mixed carboxylic-phosphorus acid derivatives of diethylenetriamine: a step towards more efficient MRI contrast agents. *Chemistry* 2003; **9**: 5899–5915.
15. Corsi DM, van der Elst L, Muller RN, van Bekkum H, Peters JA. Inulin as a carrier for contrast agents in magnetic resonance imaging. *Chemistry* 2001; **7**: 64–71.
16. André JP, Geraldes CFGC, Martins JA, Merbach AE, Prata MIM, Santos AC, de Lima JJP, Tóth É. Lanthanide(III) complexes of glycoconjugates for lectin-mediated medical imaging. *Chemistry* 2004; **10**: 5804–5816.
17. Baía P, André JP, Geraldes CFGC, Martins JA, Merbach AE, Tóth É. Lanthanide(III) chelates of DTPA bis(amide) glycoconjugates: potential imaging agents targeted at the asialoglicoprotein receptor. *Eur. J. Inorg. Chem.* 2005; 2110–2119.
18. Aime S, Botta M, Crich SG, Giovenzana G, Palmisano G, Sisti M. Novel paramagnetic macromolecular complexes derived from the linkage of a macrocyclic Gd(III) complex to polyamino acids through a squaric acid moiety. *Bioconjugate Chem.* 1999; **10**: 192–199.
19. Tóth É, Pubanz D, Vauthey S, Helm L, Merbach AE. The role of water exchange in attaining maximum relaxivities for dendrimeric MRI contrast agents. *Chemistry* 1996; **2**: 1607–1915.
20. Laus S, Sour A, Ruloff R, Tóth É, Merbach AE. Rotational dynamics account for pH-dependent relaxivities of PAMAM dendrimeric, Gd-based potential MRI contrast agents. *Chemistry* 2005; **11**: 3064–3076.
21. Aime S, Chiaussa M, Digilio G, Gianolio E, Terreno E. Contrast agents for magnetic resonance angiographic applications: ^{1}H and ^{17}O NMR relaxometric investigations on two gadolinium(III) DTPA-like chelates endowed with high binding affinity to human serum albumin. *J. Biol. Inorg. Chem.* 1999; **4**: 766–774.
22. Muller RN, Radüchel B, Laurent S, Platzek J, Piérart C, Mareski P, Vander Elst L. Physicochemical characterization of MS-325, a new gadolinium complex, by multinuclear relaxometry. *Eur. J. Inorg. Chem.* 1999; 1949–1955.
23. Aime S, Gianolio E, Terreno E, Giovenzana GB, Pagliarin R, Sisti M, Palmisano G, Botta M, Lowe MP, Parker D. Ternary Gd(III)L-HSA adducts: evidence for the replacement of inner-

Copyright © 2007 John Wiley & Sons, Ltd.

sphere water molecules by coordinating groups of the protein. Implications for the design of contrast agents for MRI. *J. Biol. Inorg. Chem.* 2000; **5**: 488–497.
24. Moghini SM, Hunter AC, Murray JC. Long-circulating and target-specific nanoparticles: theory to practice. *Pharm. Rev.* 2001; **53**: 283–318.
25. Torchilin VP, Lukyanov AN, Gao ZG, Papahadjopoulos-Sternberg B. Immunomicelles: targeted pharmaceutical carriers for poorly soluble drugs. *Proc. Natl. Acad. Sci. USA*. 2003; **100**: 6039–6044.
26. Wang J, Mongayt D, Torchilin VP. Polymeric micelles for delivery of poorly soluble drugs: preparation and anticancer activity in vitro of paclitaxel incorporated into mixed micelles based on poly (ethylene glycol)-lipid conjugate and positively charged lipids. *J. Drug. Targeting*. 2005; **13**: 73–80.
27. Mulder WJM, Strijkers GJ, van Tilborg GAF, Griffioen AW, Nicolay K. Lipid-based nanoparticles for contrast-enhanced MRI and molecular imaging. *NMR Biomed* 2006; **19**: 142–164.
28. Lanza GM, Winter PM, Hughes MS, Caruthers SD, Marsh JN, Morawski AM, Schmieder AH, Scott MJ, Fuhrhop RW, Zhang H, Hu G, Lacy EK, Allen JS, Wickline SA. Molecular imaging and therapy: new paradigms for 21(st) century medicine, polymeric drug delivery I: particulate drug carriers. *ACS Symposium Series* 2006; **923**: 295–311.
29. Kostarelos K, Emfietzoglon D. Liposomes as carriers of radionuclides: from imaging to therapy. *J. Liposome Res.* 1999; **9**: 429–460.
30. Torchilin VP, Kamenetsky MDF, Wolff GL. CT visualization of blood pool in rats by using long-circulating, iodine-containing micelles. *Acad. Radiol.* 1999; **6**: 61–65.
31. Goins B, Phillips WT, Klipper R. Blood-pool imaging using technetium-99m-labeled liposomes. *J. Nucl. Med.* 1996; **37**: 1374–1379.
32. Phillips WT, Klipper R, Goins B. Novel method of greatly enhanced delivery of liposomes to lymph nodes. *J. Pharm. Exp. Thert.* 2000; **295**: 309–313.
33. Lukyanov AN, Hartner WC, Torchilin VP. Tumor-targeted liposomes: doxorubicin-loaded long-circulating liposomes modified with anti-cancer antibody. *J. Control Release* 2004; **94**: 187–193.
34. Kellar KE, Henricks PM, Hollister R, Koenig SH, Eck J, Wei D. High relaxivity linear Gd(DTPA)-polymer conjugates: the role of hydrophobic interactions. *Magn. Reson. Med.* 1997; **38**: 712–716.
35. Duarte MG, Gil MH, Peters JA, Vander Elst L, Collet JM, Muller RN, Geraldes CFGC. Synthesis, characterization, and relaxivity of two linear Gd(DTPA)-polymer conjugates. *Bioconj. Chem.* 2001; **12**: 170–177.
36. Tóth É, Helm L, Kellar KE, Merbach AE. Gd(DTPA-bisamide)alkyl copolymers: a hint for the formation of MRI contrast agents with very high relaxivity. *Chemistry* 1999; **5**: 1202–1211.
37. André JP, Tóth É, Fischer H, Seelig A, Mäcke H, Merbach AE. High relaxivity for monomeric Gd(DOTA)-based MRI contrast agents, thanks to micellar self-organization. *Chemistry* 1999; **5**: 2977–2983.
38. Nicolle GM, Tóth É, Eisenwiener KP, Mäcke HR, Merbach AE. From monomers to micelles: investigation of the parameters influencing proton relaxivity. *J. Biol. Inorg. Chem.* 2002; **7**: 757–769.
39. Gløgård C, Hovland R, Fossheim SL, Aasen AJ, Klaveness J. Synthesis and physicochemical characterisation of new amphiphilic gadolinium DO3A complexes as contrast agents for MRI. *J. Chem. Soc., Perkin Trans.* 2000; **2**: 1047–1052.
40. Caravan P, Greenfield MT, Li X, Sherry AD. The Gd^{3+} complex of a fatty acid analogue of DOTP binds to multiple albumin sites with variable water relaxivities. *Inorg. Chem.* 2001; **40**: 6580–6587.
41. Li X, Zhang S, Zhao P, Kovacs Z, Sherry AD. Synthesis and NMR studies of new DOTP-like lanthanide(III) complexes containing a hydrophobic substituent on one phosphonate side arm. *Inorg. Chem.* 2001; **40**: 6572–6579.
42. Hovland R, Gløgård C, Aasen AJ, Klaveness J. Preparation and *in vitro* evaluation of a novel amphiphilic GdPCTA-[12] derivative: a micellar MRI contrast agent. *Org. Biomol. Chem.* 2003; **1**: 644–647.
43. Nicolle GM, Helm L, Merbach AE. ^{8}S paramagnetic centres in molecular assemblies: possible effect of their proximity on the water proton relaxivity. *Magn. Reson. Chem.* 2003; **41**: 794–799.
44. Tournier H, Hyacinthe R, Schneider M. Gadolinium-containing mixed micelle formulations: a new class of blood pool MRI/MRA contrast agents. *Acad. Radiol.* 2002; **202** (Suppl. 1): S20–S28.
45. Gløgård C, Stensrud G, Klaveness J. Novel high relaxivity colloidal particles based on the specific phase organisation of amphiphilic gadolinium chelates with cholesterol. *Int. J. Pharm.* 2003; **253**: 39–48.
46. Gløgård C. Liposomes as carriers of amphiphilic gadolinium chelates: the effect of membrane composition on incorporation efficacy and *in vitro* relaxivity. *Int. J. Pharm.* 2002; **233**: 131–140.
47. Lattuada L, Lux G. Synthesis of Gd-DTPA-cholesterol: a new lipophilic gadolinium complex as a potential MRI contrast agent. *Tetrahedron Lett* 2003; **44**: 3893–3895.
48. Kimpe K, Parac-Vogt TN, Laurent S, Piérart C, Vander Elst L, Muller RN, Binnemans K. Potential MRI contrast agents based on micellar incorporation of amphiphilic bis(alkylamide) derivatives of $[(Gd\text{-}DTPA)(H_2O)]^{2-}$. *Eur. J. Inorg. Chem.* 2003; 3021–3027.
49. Parac-Vogt TN, Kimpe K, Laurent S, Piérart C, Vander Elst L, Muller RN, Binnemans K. Gadolinium DTPA-monoamide complexes incorporated into mixed micelles as possible MRI contrast agents. *Eur. J. Inorg. Chem.* 2004; 3538–3543.
50. Accardo A, Tesauro D, Roscigno P, Gianolio E, Paduano L, D'Errico G, Pedone C, Morelli G. Physicochemical properties of mixed micellar aggregates containing CCK peptides and Gd complexes designed as tumor specific contrast agents in MRI. *J. Am. Chem. Soc.* 2004; **126**: 3097–3107.
51. Torres S, Martins JA, André JP, Geraldes CFGC, Merbach AE, Tóth É. Supramolecular assembly of an amphiphilic Gd^{III} chelate: tuning the reorientational correlation time and the water exchange rate. *Chemistry* 2006; **12**: 940–948.
52. Zettl H, Portnoy Y, Gottlieb M, Krausch G. Investigation of micelle formation by fluorescence correlation spectroscopy. *J. Phys. Chem.* 2005; **109**: 13397–13401.
53. Perez-Rodriguez M, Varela LM, Garcia M, Mosquera V, Sarmiento F. Conductivity and relative permittivity of sodium n-dodecyl sulfate and n-dodecyl trimethylammonium bromide. *Journal of Chemical Engineering Data* 1999; **44**: 944–947.
54. He X, Liang H, Huang L, Pan C. Complex microstructures of amphiphilic diblock copolymer in dilute solution. *J. Phys. Chem.* 2004; **108**: 1731–1735.
55. Sampson CB. *Textbook of Radiopharmacy, Theory and Practice*, 3rd edition. Gordon and Breach Science Publishers: London, 1999; chapter 23: 283, 294.
56. Ekeh S, Chu R, Ficken VJ, Allen EW, Ryals CJ. Distributions of perfusion and lung water. *Nucl. Med. Biol.* 1990; **17**: 561–565.
57. Frias JC, Williams KJ, Fischer EW, Fayad ZA. Recombinant HDL-like nanoparticles: a specific contrast agent for MRI of atherosclerotic plaques. *J. Am. Chem. Soc.* 2004; **126**: 16316–16317.
58. Jasanada F, Urizzi P, Suchard JP, LeGaillard F, Fabre G, Nepveu F. Indium-111 labeling of low density lipoproteins with the DTPA-bis(stearylamide): evaluation as a potential radiopharmaceutical for tumor localization. *Bioconj Chem.* 1996; **7**: 72–81.
59. Corbin IR, Li H, Chen J, Lund-Katz S, Zhou R, Glickson JD, Zheng G. Low-density lipoprotein nanoparticles as magnetic resonance imaging contrast agents. *Neoplasia* 2006; **8**: 488–498.
60. Yoshikawa K, Inoue Y, Akahane M, Shimada M, Itoh S, Seno A, Hayashi S. Phantom and animal studies of a new hepatobiliary agent for MR imaging: comparison of GdDTPA-DeA with Gd-EOB-DTPA. *J. Magn. Reson. Imaging*. 2003; **18**: 204–209.
61. Torres S, Martins JA, André JP, Pereira GA, Kiraly R, Brücher E, Helm L, Tóth É, Geraldes CFGC. $H_5EPTPACH_2OH$: synthesis, relaxometric characterization and ^{1}H NMR studies of the solution dynamics of its Ln^{III} complexes. *Eur. J. Inorg. Chem.* 2007; in press.
62. Accardo A, Tesauro D, Morelli G, Gianolio E, Aime S, Vaccaro M, Mangiapia G, Paduano L, Schillén K. High relaxivity supramole-

Copyright © 2007 John Wiley & Sons, Ltd.

cular aggregates containing peptides and Gd complexes as contrast agents in MRI. *J. Biol. Inorg. Chem.* 2007; **12**: 267–276.
63. Kabalka GW, Buonocore E, Hubner K, Davis M, Huang L. Gadolinium-labeled liposomes containing paramagnetic amphipatic agents: targeted MRI contrast agents for the liver. *Magn. Reson. Med.* 1988; **8**: 89–95.
64. Chu WJ, Simor T, Elgavish G. *In vivo* characterization of Gd(BME-DTTA), a myocardial MRI contrast agent: tissue distribution of its MRI intensity enhancement, and irs effect on heart function. *NMR Biomed.* 1977; **10**: 87–92.
65. Schuhmann-Giampieri G, Schmitt-Willich H, Press W-R, Negishi C, Weinmann H-J, Speck U. Preclinical evaluation of Gd–EOB-DTPA as a contrast agent in MR imaging of the hepatobiliary systems. *Radiology* 1992; **183**: 59–64.
66. Vittadini G, Felder E, Musu C, Tirone C. Preclinical profile of Gd-BOPTA: a liver specific MRI contrast agent. *Invest. Radiol.* 1990; **5**: S59–S60.

Copyright © 2007 John Wiley & Sons, Ltd.

DOI: 10.1002/nbm